Rev.Adv.Mater.Sci. 7 (2004) 83-90

HARDNESS EVALUATION OF NANOLAYERED PVD COATINGS USING NANOINDENTATION

J. O. Carneiro[1], V. Teixeira[1], A. Portinha[1], S. N. Dub[2] and R. Shmegera[2]

[1]University of Minho, Physics Department, GRF Group, Azurem Campus, PT: 4800-058, Guimarães, Portugal
[2]Institute for Superhard Materials, Department No.11, 2 Avtozavodskaya St., Kiev, 04074 Ukraine

Received: June 25, 2004

Abstract. The goal of the present work is to study the mechanical and structural properties of ZrO_2/Al_2O_3 nanolaminated coatings and to relate them with the nanolayered structure. ZrO_2/Al_2O_3 coatings have been grown with a nanolayered structure with 3/3.5, 6/7 and 12/14 nanometers of each layer (and with the same total thickness of 2.44 μm) using DC reactive magnetron sputtering. As substrates we have used high temperature Ni-based alloys, namely Hastelloy X. These kinds of coatings will be promissory in many technological applications where the corrosion protection combined with the wear resistance and the hard properties are required at high temperatures. Structural properties have been characterized by X-Ray Diffraction (XRD) before and after heat treatment.
Nanoindentation using a Berkovich indenter in a load range from 5 mN to 120mN was used in order to calculate the hardness and Young's modulus for the as-sputtered and heat treated coating systems. The results revealed that the hardness is almost the same for the different coatings architecture for the as-sputtered coated condition. However, after heat treatment hardness increases for all coatings and reaches 24 GPa for the ZrO_2/Al_2O_3 nanolaminated coatings prepared with 12/14 nm thickness of each layer. A detailed description of the results and their discussion will be presented in the paper.

1. INTRODUCTION

Advanced ceramic coatings applied on metallic substrates are used for high-temperature applications where a combination of strength, thermal stability and chemical inertness is needed. Ceramic coatings can be used as a protective coating to improve performance at high temperature of gas turbine components, diesel and aircraft engines. ZrO_2, or zirconia, is a ceramic material which is known to have three low-pressure structural crystalline phases: cubic, tetragonal and monoclinic. The system passes from the cubic phase to a tetragonal phase, and then to a monoclinic ground state with decreasing temperature. The cubic phase is stable (under thermodynamic point of view) between the melting temperature of 2708 °C and 2297 °C. Around 2297 °C, a transition occurs to the tetragonal phase, which is a slightly distorted version of the cubic structure and is stable between the temperature range from 2297 ºC to 1125 °C. Finally, with the following decrease in temperature, another phase transition occurs to the monoclinic phase which is thermodynamically stable below 1125 °C. This last phase transition is accomplished by a volume increase of 3-5% which promotes material damage [1]; this feature makes the use of pure zirconia in high temperature practical applications quite inapplicable. However, the cubic and tetragonal phases of zirconium oxide can be stabilized at room temperature by doping with cations such as Y^{3+}, Ca^{2+}, etc [2-5].

Fig.1 schematizes the monoclinic and tetragonal crystalline structures of zirconia. Monoclinic zirconia phase has low symmetry and a complex geometric structure with a 12-atom primitive cell. The lattice parameters are *a, b,c,* and the nonorthogonal β angle between *a* and *c*. Cubic zirconia takes the fluorite structure [1,2] in which the Zr atoms are in a

Corresponding author: J. O. Carneiro, e-mail: carneiro@fisica.uminho.pt

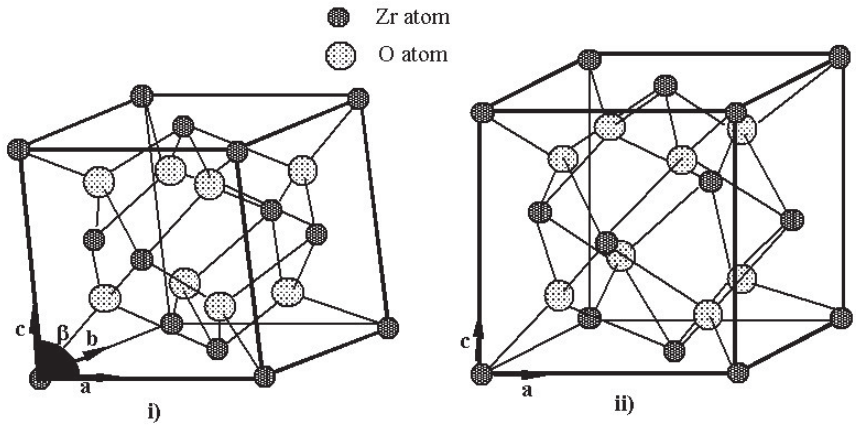

Fig.1. Monoclinic and tetragonal crystalline structures of Zirconia.

face-centered-cubic (*fcc*) structure and the oxygen atoms occupying the tetrahedral sites are associated with the *fcc* lattice. The zirconia tetragonal phase can be viewed as a distortion of the cubic structure if alternating pairs of oxygen atoms are displaced up and down in the vertical direction.

Besides this mechanism, two other approaches can be employed to retain the high temperature tetragonal phase: mixing ZrO_2 with an oxide such as Al_2O_3 [3,6] and decreasing the particle size of the crystalline domains, i.e., using small zirconia crystals with radii lower than 6 nm (the surface energy of the tetragonal phase is lower than that of the monoclinic phase; it results in stable tetragonal crystal at room temperature) [7,8]. Zirconia – alumina (ZrO_2/Al_2O_3) nanolaminate thin coatings are a material solution to stabilize thermally the zirconia high-temperature tetragonal phase at room temperature. The ZrO_2/Al_2O_3 bulk composite is a classic model of the transformation-toughening ceramic system. Al_2O_3 is not soluble with ZrO_2 and alters the stability through constraint. Alumina has a Young's modulus higher than zirconia and it is suggested that it forms a rigid matrix around the zirconia crystals which causes a local compressive stress and hinders the *Umklapp* mechanism of the martensic phase transformation [6].

It is well known that coatings mechanical properties are related not only with an intrinsic stress generated during physical vapour deposition (PVD) caused by high energetic particle bombardment, chemical reactions, phase transformation, *etc.*, but also by the thermoelastic effects – thermal stress due to a mismatch between substrate and coating coefficient of thermal expansion (CTE). One of the effective ways to accede the mechanical properties of thin films (even in a nanometer scale) is the nanoindentation technique. The nanoindentation technique consists of measurements of load – displacement curves that allows the assessment of hardness and elastic modulus values. According to a definition attempt of Martens [9], hardness is understood as the resistance of a body against penetration of a second body. This simple definition collides with the necessity to quantify hardness as a physical unit. Impression hardness is derived from an indentation test: a body of standard geometry is impressed into the specimen, and, after the test, the area *A* of the generated deformation is used to characterize the hardness. The Vickers test uses a four-sided pyramid, Brinell hardness is based on impression of spheres and Berkovich uses a three sided pyramid [10]. In this work we used the Berkovich indenter since it is preferred to the Vickers because of the difficulty in grinding the four-sided Vickers to terminate at a point.

2. NANOINDENTATION THEORETICAL CONSIDERATIONS

Nanoindentation process is one of the mechanical tests available to provide information about the mechanical properties of thin films. The advantages of nanoindentation technique are numerous, as nanoindentation load-displacement data contain a wealth of information. The technique measures the coating hardness, gives the coating elastic modulus, E_f (Young's modulus) from the same data [11,12]

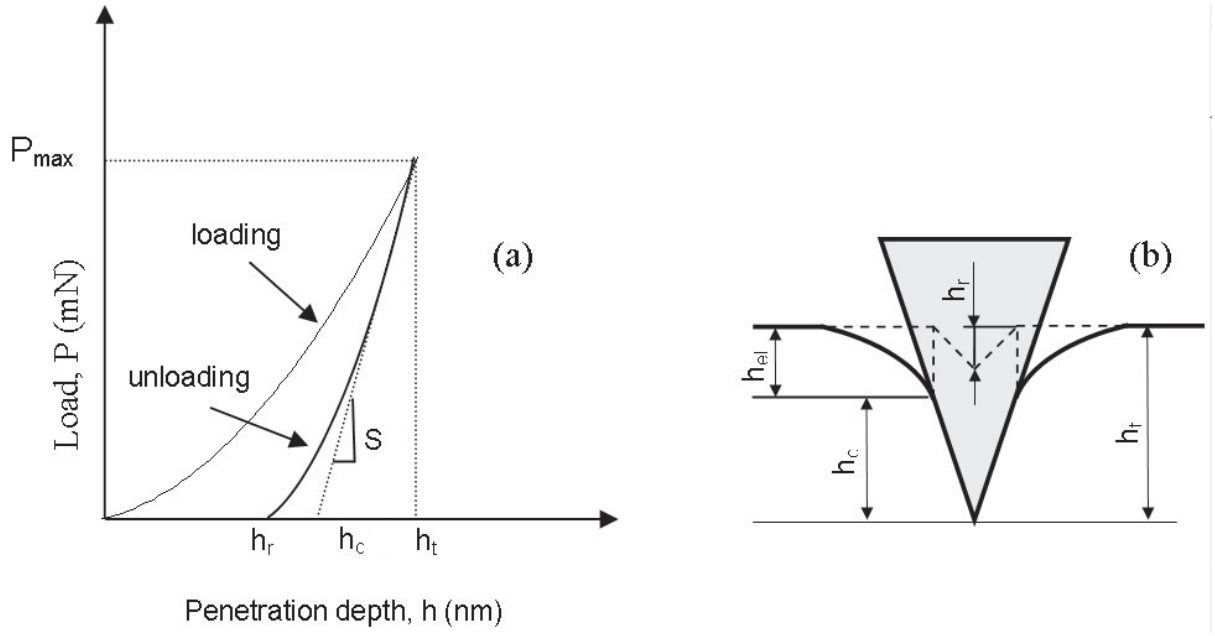

Fig.2. (a) Load-displacement curve of a loading/unloading cycle with localisation of the characteristic penetrations h_r, h_c and h_t on the depth scale; (b) schematic representation of the deformation under maximum peak load with characteristic depths h_t (maximum depth) and h_c (contact depth); and situation after complete unloading with residual depth h_r.

both free from substrate effects even for coatings of a few sets of ten nanometers.

The characteristic impression geometry and the resulting load-displacement curve are displayed in Fig. 2. Under full load, the indenter is impressed to a total depth h_t, which can be taken from the load-displacement curve. After complete unloading, a remaining depression of depth h_f is left. The value of h_r is also contained in the load-depth curve. However, the contact depth h_c is required for Meyer hardness calculation [13]. The contact area A_c will be obtained by cutting the indenter in a height h_c from its tip, and the Meyer hardness or the mean contact pressure is given by

$$H = \frac{P_{max}}{A_c}, \tag{1}$$

where P_{max} is the maximum peak load and A_c is the projected contact area at this load, and

$$E_r = \frac{\sqrt{\pi}}{2}\frac{2}{\sqrt{A}}, \tag{2}$$

where E_r is the reduced elastic modulus which account for the fact that elastic displacements occur in both indenter and the sample, and $S = dP/dh$ is the initial unloading contact stiffness (i.e., the slop of the initial portion of the unloading curve). The elastic modulus of the test material, E, is calculated from E_r using

$$\frac{1}{E_r} = \frac{1-\nu_f^2}{E_f} + \frac{1-\nu_i^2}{E_i}, \tag{3}$$

where ν_f is the Poisson's ratio for the test material, and E_i and ν_i are the elastic modulus and Poisson's ratio of the indenter, respectively. For diamond, the elastic constants E_i = 1141 GPa and ν_i = 0.07 [14].

The basic parameters calculated from the load-displacement curves are the peak load, P_{max}, the displacement at peak load, h_t, the initial unloading contact stiffness, S. The calculation of h_c needs theoretical model assumptions following from the indenter geometry. However, the contact depth is estimated as follows:

$$h_c = h_t - \varepsilon\frac{P_{max}}{S}, \tag{4}$$

Table 1. Structure of individual layers and coating thickness for the (ZrO_2/Al_2O_3) nanolaminated coatings.

Sample structure	ZrO_2/Al_2O_3	ZrO_2/Al_2O_3	ZrO_2/Al_2O_3
Sample code	Zr3/Al3.5	Zr6/Al7	Zr12/Al14
Number of layers	375/375	188/188	94/94
Layer thickness, (nm)	3/3.5	6/7	12/14
Bi-layer thickness, (nm)	6.5	13	26
Total thickness, (mm)	2.44	2.44	2.44

where $\varepsilon = 0.75$ for a Berkovich indenter. At a last step of the analysis, the projected contact area is calculated by evaluation an empirically determined indenter area function $A_c = 24.56\, h_c^2$.

In order to obtain the instantaneous contact depth, it is necessary to subtract the elastic deflection from each displacement measurement registered during the test. Many commercial nanoindentation testing systems have available software that enables to measure the stiffness in a continuous way. However, our Nano Indenter II has no continuous stiffness option. To monitor the average contact depth in the indent during reloading of the indenter, the procedure suggested by Novikov and Dub [15-16] was used. The basis of this approach is the equation that relates the elastic displacement h for simple punch geometries to the load peak, $P = \alpha\, h^m$ [17], where α and m are constants. From the above relation, it follows that the current value $h_{(el)i}$ of elastic deflection for the sample surface at contact perimeter is

$$h_{(el)i} = h_{(el)max}\left(\frac{P_i}{P_{max}}\right)^{\frac{1}{2}}, \qquad (5)$$

where P_i is the instantaneous applied load during the nanoindentation test and $h_{(el)max}$ is the elastic surface deflection at the maximum load [i.e. $h_{(el)max} = (h_t - h_c)$]. At each deep indentation point the instantaneous contact depth is

$$(h_c)_i = (h_t)_i - h_{(el)i}. \qquad (6)$$

So, from Eq. (6), it is now possible to calculate $(h_c)_i$ for each deep indentation position and then the instantaneous area function $(A_c)_i = 24.56\,(h_c)_i^2$. Finally, using Eq. (1), the instantaneous hardness can be obtained changing P_{max} by P_i and A_c by $(A_c)_i$; that is

$$(H_i) = \frac{P_i}{24.56\left[(h_t)_i - 0.75\left(\frac{P_{max}}{S}\right)\left(\frac{P_i}{P_{max}}\right)^{\frac{1}{2}}\right]^2}. \qquad (7)$$

3. EXPERIMENTAL DETAILS FOR NANOLAYERED COATINGS

The nanocomposite (ZrO_2/Al_2O_3) coatings composed of nanolayers (3/3.5, 6/7 and 12/14) nanometers (assigned as *ZrxAly* codes, where *x* and *y* are the different thicknesses for ZrO_2 and Al_2O_3, respectively) have been deposited by DC reactive magnetron sputtering from high pure metallic targets (Zr and Al) in order to stabilize the high temperature tetragonal phase of zirconia at room temperature. We have used high temperature Ni-based alloys, namely Hastelloy X, as substrates. Details about the PVD coatings preparation are described elsewhere [18]. The structure and thickness of the coatings are presented in Table 1.

After PVD deposition, the coatings were subjected to 20 thermal cycles in air from 600 °C to 1000 °C using the solar furnace of the Solar Platform of Almeria (PSA), in Spain.

Structural properties and residual stresses of the PVD as-sputtered and heat treated coatings were obtained from X-ray diffraction (XRD) using a Philips PW-1710 diffractometer operating with Cu$K\alpha$ (40 kV, 20 mA) radiation with the 2θ angles in the range 20-70° with the steps of 0.02°. Hardness was evaluated by Nanoindentation with a Nano Indenter II (MTS Systems, Oak Ridge, USA) using a Berkovich indenter. Five indents were performed for each sample and for four different loads (5mN, 30mN, 50 mN, and 120 mN).

4. RESULTS AND DISCUSSION

4.1 Structural properties

The structural properties of the sputtered coatings were analysed by XRD in order to study the phases of the nanolaminated coatings and grain sizes in the as-sputtered and heat treated conditions.

Fig. 3 presents the results of XRD measurements. For the nanolaminated coatings with (3/3.5) nanometer layer thicknesses of (ZrO_2/Al_2O_3) system, we observe that it has a quasi-amorphous X-

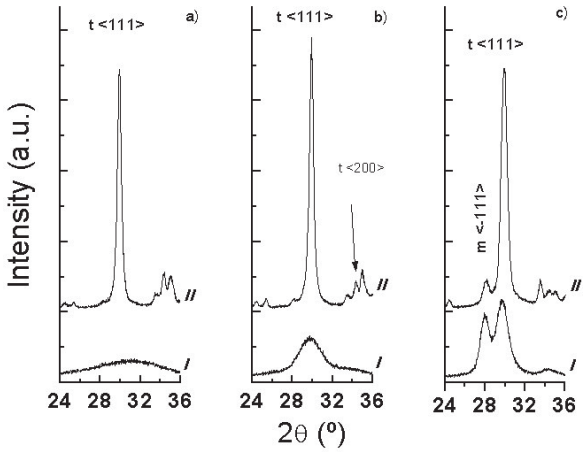

Fig. 3. X-Ray difraction patterns of nanolaminated coatings, (*I*) as-sputtered and (*II*) heat treated; (a) sample with 3/3.5 nm thickness in each layer of ZrO_2/Al_2O_3, respectively, (b) sample with 6/7 nm thickness in each layer of ZrO_2/Al_2O_3, respectively, (c) sample with 12/14 nm thickness in each layer of ZrO_2/Al_2O_3, respectively.

ray structure which evidence the tetragonal phase. For higher nanolayer thicknesses (6/7 and 12/14), the tetragonal phase is found clearly with the (111) crystallographic plane parallel to the interface. The tetragonal zirconia (111) planes are the most densely packed and, for this reason, they are thermodynamically favored to grow parallel to the substrate. It is well known that alumina is not soluble with zirconia and according to Lange [19] alters the stability through constraint. Lange theory shows that the structural stability of tetragonal zirconia depends essentially on the critical nucleus size that is decreased by a constraining matrix having an elastic modulus higher than that of ZrO_2 (this is the case for Al_2O_3). The stable tetragonal zirconia phase is produced when each zirconia layer thickness is less than the radius at which an unconstrained, unstressed hemispherical tetragonal zirconia crystallite spontaneously transforms to monoclinic at the growth temperature [20].

The produced ZrO_2 nanolaminate coatings with nanolayer thicknesses of 3, 7 and 12 nm are in good agreement with those derived by Aita *et al.* using an end-point thermodynamics analysis and the following expression for the critical radius R_c at which a tetragonal-to-monoclinic zirconia growth transformation occurs

$$R_c = 3.79\,[1 - (T/1448)]^{-1}\ \text{nm}, \qquad (8)$$

Table 2. Grain sizes obtained from X-ray diffraction analysis.

		Sample Code		
		Zr3Al3.5	Zr6Al7	Zr12Al14
Grain Size (nm)	*As-Sputtered*	4.9	7.3	12.8
	Heat Treated	17.8	18.2	11.2

where T is the deposition temperature in Kelvin (K). At the growth temperature used in our experiments, Eq. (8) gives a critical radius R_c = 6.3 nm. In fact, the samples with the ZrO_2 layer thickness of 12 nm present some monoclinic grains in the tetragonal matrix (see Fig. 3). The estimation of the nanocrystallite size of the zirconia-alumina multilayer films by the XRD peak broadening indicates that they have an average crystallite dimension approximately equal to the nanolayer thickness, as can be seen in Table 2.

A quasi-amorphous or tetragonal phase is retained at room temperature for layer thicknesses lower than 12 nm. In this study, heat treatment experiments were performed in order to study the ZrO_2 tetragonal phase stability. As can be observed from Fig.3 (*II*) all coatings crystallize in tetragonal phase after heat treatment. However, the traces of the monoclinic phase in *m*(-111) direction remains for ZrO_2 with 12 nm layer thickness. As for the grain size, we have measured higher grain sizes after heat treatment for (3/3.5 and 6/7) structures; nevertheless, a small grain size decrease was measured for the (12/14) structure.

4.2 Mechanical properties: residual stress and nanoindentation

The residual stresses of the as-deposited PVD coatings were obtained using the deflection technique (DTq) by measuring the curvature or deflection of the substrate before and after coating deposition. The residual stress value, s_r is determined by Stoney's equation [21] using substrate curvature radii, both before and after coating deposition. To obtain this curvature radius, a micro-displacement laser transducer with a resolution of 0.2 μm was used. The data points were fitted to a parabolic equation in order to obtain the curvature substrate radius [22]. The in-plane surface residual strain/stress in

Table 3. Residual stress values obtained from XRD and deflection techniques.

Residual Stress (GPa)	Sample Code		
	Zr3Al3.5	Zr6Al7	Zr12Al14
As-Sputtered (DTq)	0.5	-0.4	-0.2
Heat Treated (XRD)	-3.4	-3.8	-4.2

the coatings after heat treatment was evaluated by XRD technique [23]. Table 3 summarizes the residual stress values obtained from XRD and deflection techniques.

Generally, the residual stresses in the as-sputtered coatings have small magnitudes. However, all coatings have changed to a high compressive stress state after heat treatment. This increase in compressive stress is due to the stress related with the coating thermal stress component because of a mismatch in the coefficients of thermal expansion (CTE) of the substrate and coating.

The indentation hardness is not a fundamental material property, but depends on the way it is obtained (testing technique, evaluation, *etc*.). Nevertheless, the nanoindentation hardness is widely used as a parameter characterizing the mechanical properties of materials, in particular, for thin coatings. In fact, nanoindentation hardness tests are relatively easy to perform and provide a value that can give a direct measure for the film loading – bearing capacity without substrate effects. The nanoindentation response for as-sputtered and heat treated films made at 30 mN peak indentation load is shown in Fig. 4a for the Zr*12*Al*14* samples. For both situations, the depth dependence on hardness is shown in Fig. 4b according Eq. (7).

As seen from Fig.4a, the heat treated Zr*12*A1*4* shows a stiffer plastic response, which manifests itself in the greater loading parabolic curvature. This response results in a smaller indentation area for the same maximum load, suggesting that the material is more resistant to plastic deformation. In fact, if an indented material is in a higher compressive residual stress state, the indenter will penetrate the material less deeply for a given applied load. This qualitative analysis is consistent with XRD residual stress results presented in Table 3. In addition, the results presented in Fig.4b also show a hardness

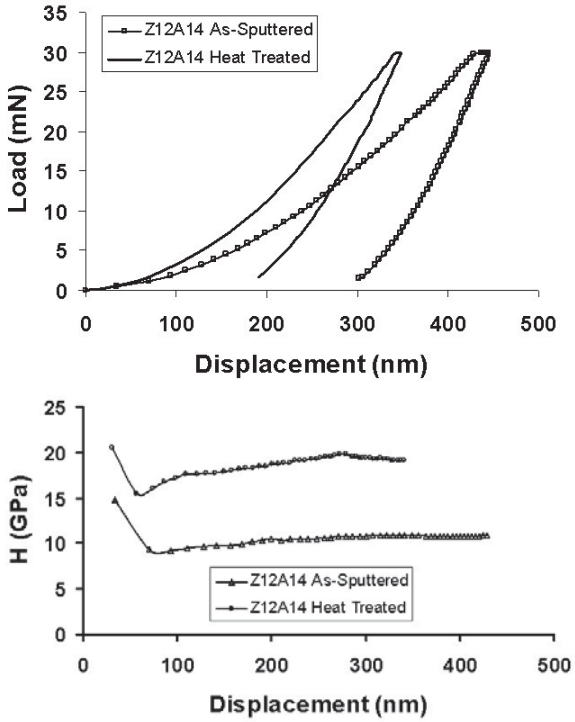

Fig.4. (a) Load-displacement data during one complete cycle of loading and unloading (b) variation of nanoindentation hardness with indenter depth for the tested samples *Zr12A14.*

increase for Zr*12*A1*4* sample after heat treatment. It can also be observed that, in general, a substrate effect was not detected for both conditions since hardness is almost constant in spite of the increase in indenter displacement. All coatings have shown a similar behaviour. It is important to refer that similar curves were obtained using higher peak loads, but coating hardness begins to decrease due to the softer substrate effect. Fig. 5 shows the experimentally nanoindentation hardness, *H*, for all studied coatings as a function of the maximum peak load.

It can be observed from Fig. 5 that the hardness decreases with increasing peak loads for all coatings and for both conditions (as-sputtered and heat treatment). The hardness changes are small for the test performed with peak loads of 5 and 30 mN. However, when the peak load is raised up to 50 mN, a substantial hardness decrease is observed which evidences the substrate effect. Actually, the substrate used in this work is softer than the deposited films which justify the hardness decreasing.

The values of hardness and coating elastic modulus, both calculated from the loading-displacement data corresponding to the nanoindentation test performed at 30 mN peak load are plotted in Fig. 6. For

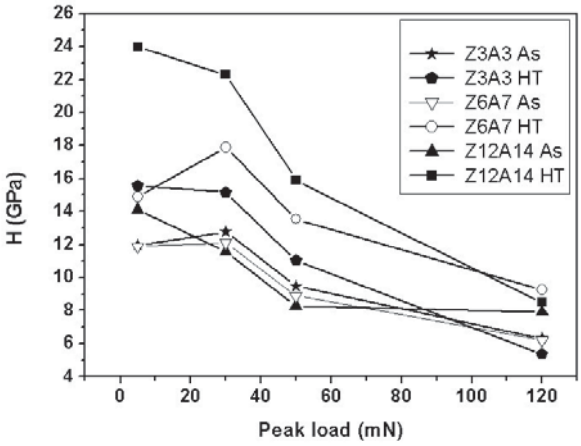

Fig.5. Variation of nanoindentation hardness with the peak load for the different coatings (The letters after code sample means: As: as-sputtered and HT: heat treated).

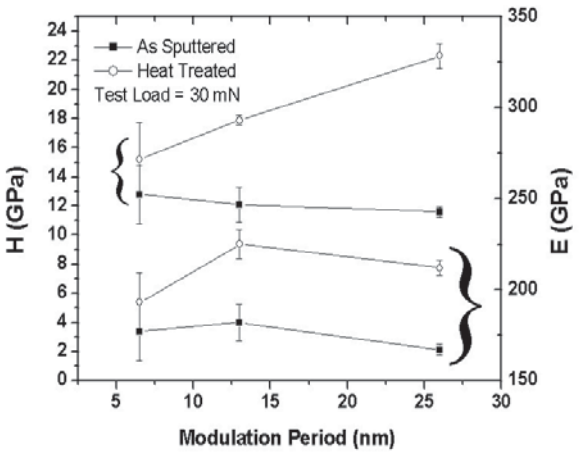

Fig.6. Hardness and elastic modulus evolution with modulation period for all coatings (as-sputtered and heat treated).

the as-sputtered condition, both hardness and elastic modulus have decreased slightly for higher modulation periods (i.e. sum of the ZrO_2 and Al_2O_3 nanolayer thicknesses).

The decrease in hardness values agrees with the theory since it is expected that hardness decreases for higher bi-layer thicknesses (i.e. *modulation periods*) and grain sizes (see also Table 1). The fact that hardness increases for lower grain size is in accordance with other studies [24-27], where the increase in number of grain boundaries was shown to be the reason of the increase in the surface energy and for the slowing of the dislocations propagation.

Both hardness and elastic modulus have increased after the heat treatment. It is well known that the material properties determine their usefulness. The elastic modulus is an important material mechanical property that can be viewed as being related to stiffness: the higher is the value of *E*, the stiffer is the material. Nevertheless, high stiffness does not means a high ability of a material to be deformed or capacity to absorb energy without rupture. For example, brittle materials are strong but have poor deformation capacity. This explanation is in a good agreement with the experimental results shown in Figs. 4a and 6. It can be seen that hardness values obtained for the as-sputtered coatings do not differ so much from one to another, but, a significant increase is observed after the heat treatment. However, the hardness values increases with the increase in the modulation periods too; in particular, the increase in hardness is much more pronounced for Zr*12*A*14* coating, it reaches a magnitude that is almost double (≈ 24 GPa) than the untreated one.

5. CONCLUSIONS

We have deposited nanosized laminates of ZrO_2-Al_2O_3 by DC reactive magnetron sputtering in order to stabilize the zirconia high temperature tetragonal phase at room temperature. Each layer thickness was scaled to ensure that zirconia grains are nanosized and thus promoting the transformation-toughening effect. After heat treatment, the quasi-amorphous tetragonal zirconia samples with nanosized grains crystallizes to tetragonal phase without any monoclinic transformation at nanolayer thicknesses lower than the radius at which an unconstrained tetragonal zirconia crystallite spontaneously transforms to monoclinic at the growth temperature (approximately 6.3 nm). However, for samples with (12/14) nanolayer thicknesses, traces of the monoclinic phase were still retained. It was also shown that the residual stresses are dependent on the ZrO_2-Al_2O_3 nanolaminate thicknesses. Heat treatment allows the stresses to be relaxed at high temperature such that, on cooling down to room temperature, an in-plane biaxial compressive stress will be arised not only due to the difference in CTE between the substrate and the nanolaminates, but also due to the alumina matrix constraining effect.

Concerning the coating mechanical properties, it has been shown from experimental studies that the mechanical properties of the ZrO_2/Al_2O_3

nanolayered structure can be quantified through experimental nanoindentation tests. The experimental results revealed that for the as-sputtered coated systems hardness is almost the same for the different coatings architecture. However, after heat treatment, hardness increases for all coatings and reaches 24 GPa for a ZrO_2/Al_2O_3 nanolaminated coatings prepared with 12/14 nm thickness of each layer. The elastic modulus for as-deposited samples is almost constant for different coatings architectures (≈ 170 GPa). The *E* value has increased approximately to 200 GPa after heat treatment due to a sintering process.

It was also observed that nanoindentation experiments carried out at lower peak load magnitudes gives the true coating mechanical behaviour since a substrate effect is not detected here.

ACKNOWLEDGEMENTS

This work was financially supported by FCT-Fundação para a Ciência e Tecnologia- under the project POCTI/EME/39316/2001: 'PVDCOAT-Composite and multilayered protective coatings for efficient energy systems'.

The authors are gratefully for the exchange programme and use of Solar Furnace facility through the European project EC-5FWP-PSA-Industrial Applications of Solar Thermal Energy- Improving Human Potential Programme/2002. *'Solar furnace for high temperature treatment of advanced composite ceramic coatings'*.

REFERENCES

[1] Robert A. Miller // *Surface and Coatings Technology* **30** (1987) 13.
[2] V. Teixeira, M. Andritschky, W. Fischer, H. P. Buchkremer and D. Stöver // *Surface and Coatings Technology* **120-121** (1999) 103.
[3] V. Teixeira and M. Andritschky // *High Temperature-High-Pressures* **25** (1993) 213.
[4] H. G. Scott // *J. Mat. Sci*. **10** (1975) 15227.
[5] P. Gao, L. J. Meng, M.P dos Santos, V. Teixeira and M. Andritschky // *Applied Surface Science* **173** (2001) 84.
[6] S. B. Qadri, C. M. Gilmore, C. Quinn, E. F. Skelton and C. R. Gosset // *J. Vac. Sci. Technol*. *A* **7** (1989) 1220.
[7] B. E. Yoldas // *J. Mat. Sci*. **21** (1986) 1080.
[8] C. R. Aita, M. D. Wiggins, R. Whig, C. M. Scanian and M. Gajdardziska-Josifovska // *J. Appl. Phys*. **79** (1996) 1176.
[9] *A. Handbuch der Materialkunde für den Maschinenbau* (Springer, Berlin, 1898) p. 234.
[10] M. Klein, *Einführung in die DIN-Normen* (Teubner Verlag, Stuttgart, 1997).
[11] M. F. Doerner and W. D. Nix // *J. Mater. Res.* **1** (1986) 43.
[12] W. C. Olivier and G. M. Pharr // *J. Mater. Res.* **7** (1992) 1564.
[13] E. Meyer // *Zeitschrift Verein Deutscher Ingenieure* **52** (1908) 645, in German.
[14] G. Simmons and H. Wang, *Single Crystal Elastic Constant and Calculated Aggregate Properties: A Hanbook 2nd ed* (The M.I.T. Press, Cambridge, Massachusetts, 1971).
[15] S. Dub, N. Novikov and Y. Milman // *Phil. Mag. A* **82** (2002) 2161.
[16] N. V. Novikov, S.N. Dub, Yu. V. Milman, I.V. Gridneva and S.I. Chugunova // *J. Superhard Mater.* **3** (1996) 32.
[17] H. E. Boyer and T. L. Gall, *Metals Handbook* (American Society for Metals, Metals Park, Ohio, 1985).
[18] V. Teixeira, A. Monteiro, J. Duarte and A. Portinha // *Vacuum* **67** (2002) 477.
[19] F. F. Lange // *J. Mat. Sci* **17** (1982) 225.
[20] M. Gajdardziska-Josifovska and C. R. Aita // *J. Appl. Phys.* **79** (1996) 1996.
[21] G.G. Stoney // *Proc. R. Soc. (Lond.) A* **82** (1909) 172.
[22] P.M. Ramsey, H. W. Chandler and T. F. Page // *Surf. Coat. Technol*. **43-44** (1990) 223.
[23] I. C. Noyan and, J. B. Cohen, *Residual Stress: measurement by X-ray diffraction and interpretation* (Springer Verlag, Berlin, 1987).
[24] R. Venkatraman, J.C. Bravman, W. D. Nix. P. Davies, P.A. Flinn and D.B.J. Fraser // *Electron. Mater.* **10** (1990) 1231.
[25] M. Kobrinsky and C.V. Thompson // *Acta Mater.* **48** (2000) 625.
[26] E. Chu, Y.L. Shen and S. Suresh, *Lexcom Report* (Massachusetts Institute of Technology, Cambridge, MA, 1996).
[27] A. Portinha, V. Teixeira, J. Carneiro, S.N. Dub and R. Shmegera // *Rev. Adv. Mat. S*ci **5** (2003) 311.